RSC Advances

PAPER

View Article Online
View Journal | View Issue

Cite this: *RSC Adv.*, 2019, **9**, 878

Facile solvothermal preparation of Fe_3O_4–Ag nanocomposite with excellent catalytic performance

Fangke Zhan,[a] Ran Wang,[a] Juanjuan Yin,[a] Zengsheng Han,*[a] Lun Zhang,[a] Tifeng Jiao,*[ab] Jingxin Zhou,[a] Lexin Zhang[a] and Qiuming Peng[b]

Functional nanocomposites demonstrate excellent comprehensive properties and outstanding characteristics for numerous applications. Magnetic nanocomposites are an important type of composite materials, due to their applications in optics, medicine and catalysis. In this report, a new Fe_3O_4-loaded silver (Fe_3O_4–Ag) nanocomposite has been successfully synthesized *via* a simple solvothermal method and *in situ* growth of silver nanowires. The silver nanowires were prepared *via* the reduction of silver vanadate with the addition of uniformly dispersed Fe_3O_4 nanoparticles. Structural and morphological characterizations of the obtained Fe_3O_4–Ag nanocomposite were carried out using many characterization methods. As a new composite catalyst, the synthesized magnetic Fe_3O_4–Ag nanocomposite displayed a high utilization rate of catalytically active sites in catalytic reaction medium and showed good separation and recovery using an external magnetic field. The facile preparation and good catalytic performance of this Fe_3O_4–Ag nanocomposite material demonstrate its potential applications in catalytic treatment and composite materials.

Received 15th October 2018
Accepted 21st November 2018

DOI: 10.1039/c8ra08516a

rsc.li/rsc-advances

1. Introduction

In recent years, the pollution of water by phenol and aniline compounds has attracted widespread attention worldwide. Among these compounds, 4-nitrophenol (4-NP) belongs to a class of highly toxic compounds, which are difficult to degrade and most difficult to treat. At the same time, 2-nitroaniline (2-NA) has strong water solubility, and can easily penetrate into the soil. The polluted soil then causes pollution of surface water, groundwater and river water. Thus, nitroaniline substances have been listed as key environmental pollutants in many countries. In order to efficiently degrade 2-NA and 4-NP, various nanomaterial catalysts, such as CuO,[1] Ag/KCC-1,[2] and CuPd,[3] have been successfully developed. In particular, among these materials, magnetic nanoparticles have shown great potential in the degradation and catalysis of organic pollutants. Fe_3O_4 has aroused great research interest in the field of magnetic materials and its wide applications are well established[4] in fields such as magnetic resonance imaging (MRI),[5] spintronics,[6,7] lithium ion batteries,[8] catalysis,[9] targeted drug delivery[10,11] and environmental remediation.[12–14] Metal nanoparticles also have many applications, in fields such as catalysis, electronics, optics, optoelectronics, sensing and data storage. Because of their unique properties,[15–26] metal nanoparticles represent an important class of components. Ag nanoparticles exhibit many original chemical, physical and catalytic properties as good metal conductors.[27] In recent years, self-assembled Ag composite materials have attracted the increasing attention of a large number of scientific researchers, including those in fields such as high-performance nanofilms,[28] biosensors,[29] electroless copper plating[30] and catalytic materials.[31–33] Thus, in the present work, Ag nanoparticles were speculated to form a magnetic nanocomposite with Fe_3O_4 particles, which could be expected not only to show good catalytic performance, but also reduce the loss of Ag nanoparticles and increase reusability.

In this work, Fe_3O_4 nanoparticles with uniform and controllable sizes were prepared using a modified solvothermal method. Then a uniform Fe_3O_4–Ag nanocomposite was successfully prepared and characterized by a series of morphological and spectral characterization techniques. The obtained Fe_3O_4–Ag composite was used as a new catalyst for catalytic reduction reactions of 4-NP and 2-NA, demonstrating good catalytic ability and excellent reusability.

2. Materials and methods

2.1 Materials

Ferric chloride hexahydrate ($FeCl_3 \cdot 6H_2O$) and polyethylene glycol (PEG, M_w ~6000 g mol^{-1}) were purchased from Aladdin

[a]Hebei Key Laboratory of Applied Chemistry, School of Environmental and Chemical Engineering, Yanshan University, Qinhuangdao 066004, China. E-mail: hanzs@ysu.edu.cn; tfjiao@ysu.edu.cn

[b]State Key Laboratory of Metastable Materials Science and Technology, Yanshan University, Qinhuangdao 066004, China

Reagent (Shanghai, China). Ethanol (C_2H_5OH, analytical reagent) was provided by Sinopharm Chemical Reagent Co., Ltd (Beijing, China). Ethylene glycol ($C_2H_6O_2$), silver vanadate, and oleylamine were purchased from Alfa Aesar (Beijing, China). Sodium borohydride ($NaBH_4$), sodium hydroxide (NaOH), 4-nitrophenol (4-NP, 99%) and 2-nitroaniline (2-NA, 99%) were obtained from Alfa Aesar (Beijing, China). Ultra-pure water was obtained using a Milli-Q Millipore filter system (Millipore Co., Bedford, MA, USA) with a resistivity of 18.2 MΩ cm^{-1}. All chemicals were used without further purification.

2.2 Fabrication of Fe_3O_4–Ag nanocomposite

The synthesis of the Fe_3O_4–Ag nanocomposite was obtained according to the following procedure. Briefly, 1.35 g of ferric chloride hexahydrate ($FeCl_3 \cdot 6H_2O$) was put into 30 mL of ethylene glycol ($C_2H_6O_2$) to form a dispersed solution. Then 1.0 g of polyethylene glycol (PEG) and 0.8 g of sodium hydroxide (NaOH) were added to the above solution. The above mixed solution was stirred for 30 minutes and transferred into a Teflon-lined stainless-steel autoclave (~100 mL) for next reaction, which took place for 8 h under a temperature of 180 °C. After completion of the reaction, the black precipitate (*i.e.*, Fe_3O_4 nanoparticles) was collected using a magnetic block, and washed with deionized water and ethanol repeatedly, followed by drying at 60 °C in a vacuum oven.[34] 0.635 g of silver vanadate powder and 10 mL of oleylamine were transferred into a 50 mL flask filled with nitrogen gas for a repeated 3 times at room temperature. Then the reaction system was magnetically stirred for 24 hours until the liquid turned from transparent to bright yellow. After this, 2.5 mL of the silver vanadate/oleylamine mixed solution was dropwise added to 40 mL of the Fe_3O_4 suspension solution (1 mg mL^{-1}) in *n*-hexane. Then the reaction was continued for 2 h at 70 °C under strong nitrogen agitation and mechanical stirring. The final product was magnetically separated and washed 3 times with ethanol.[35]

2.3 Catalytic performance test

In order to investigate the catalytic performance of the obtained Fe_3O_4–Ag nanocomposite, we selected 4-NP and 2-NA as model molecules to characterize the process.[36–45] In the catalytic experiments, fresh $NaBH_4$ (20 mL, 0.01 M) solution was added to 2-NA or 4-NP solution (2 mL, 5 mM) at room temperature. $NaBH_4$ was used as a reducing agent for this catalytic reduction reaction. The Fe_3O_4–Ag composite (10 mg) was added into ethanol (10 mL) to form a stable suspension solution. Then the obtained Fe_3O_4–Ag composite suspension (300 μL, 1.0 mg mL^{-1}) was added to the 2-NA or 4-NP solution to catalyze the reduction reaction. The progress of this catalytic reaction was monitored using UV-vis spectroscopy at room temperature. For the next recycling experiment, the used F_3O_4–Ag composite was recovered by magnetic separation, and was then washed with deionized water and ethanol thoroughly several times. The catalytic process was repeated for 8 consecutive cycles using the same solid powder with new fresh 4-NP/2-NA and $NaBH_4$ aqueous solutions.

2.4 Characterization

The prepared nanocomposite material was treated to remove water with a freeze dryer at −48 °C for 48 h using a FD-1C-50 instrument (Beijing Boyikang Experimental Instrument Co., Ltd., China). The morphologies were characterized using transmission electron microscopy with an accelerating voltage of 20 kV (TEM, HT7700, Hitachi High-Technologies Corporation, Japan). The structure of the Fe_3O_4–Ag composite was investigated using a field-emission scanning electron microscope (SEM, S-4800II, Hitachi, Japan) with an accelerating voltage of 5–15 kV. X-ray diffraction (XRD) characterization was performed using a Rigaku D/max 2550PC diffractometer (SMART LAB, Rigaku, Japan). The XRD patterns were obtained using Cu Kα X-ray radiation with an incident wavelength of 0.1542 nm and current of 200 mA under a voltage of 40 kV. The magnetic properties of the products were characterized using a vibrating sample magnetometer (VSM) of the Physical Property Measurement System (PPMS, Quantum design Model 6000) magnetometer (MPMS-XL, Quantum Design Inc. San Diego, CA, USA) at 300 K. HRTEM photographs were obtained using an FEI Tecnai F20 electron microscope operating at 200 kV (FEI Trading (Shanghai) Co., Ltd, China). X-ray photoelectron spectroscopy (XPS) was performed using a Bragg diffraction setup (SMART LAB, Rigaku, Japan) with an Al Kα X-ray source.

3. Results and discussion

3.1 Characterization of Fe_3O_4–Ag nanocomposite

Fig. 1 demonstrates the schematic synthesis process of the Fe_3O_4–Ag nanocomposite. Firstly, magnetic Fe_3O_4 nanoparticles with well-defined geometries were synthesized using a modified solvothermal method.[46–48] It was found that the initial geometry of the Fe_3O_4 nanoparticles changed with the addition of an initial mass of NaOH.[34] After that, the multifaceted geometry of the Fe_3O_4 nanoparticles was covered with *in*

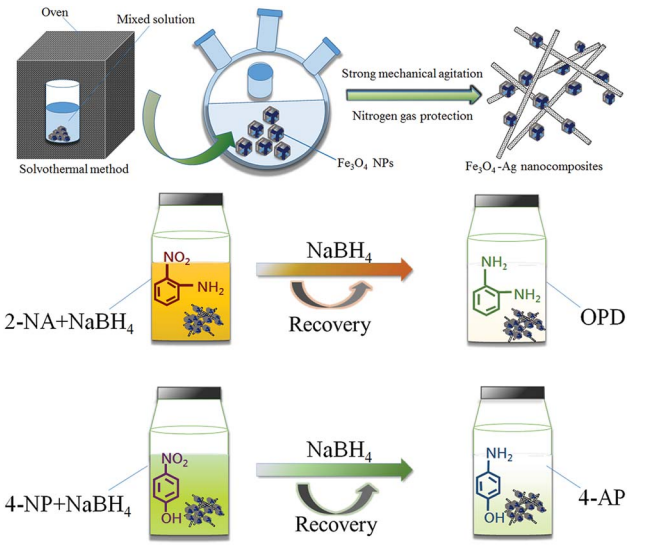

Fig. 1 Schematic illustration of the preparation and catalytic performances of the obtained Fe_3O_4–Ag nanocomposite.

situ grown silver nanowires. In the process of oleylamine reducing silver vanadate, Ag nanowire crystals grew *in situ* in the presence of the Fe_3O_4 nanoparticles under strong mechanical agitation. Then, the scheme illustrates the catalytic reaction of the Fe_3O_4–Ag nanocomposite with the substrates 4-NP and 2-NA. More specifically, 4-NP was reacted with fresh $NaBH_4$ solution to obtain the product 4-aminophenol (abbreviated as 4-AP). Similarly, in the presence of the Fe_3O_4–Ag nanocomposite, the reduction process showed the conversion of the reactant 2-nitroaniline to *o*-phenylenediamine (abbreviated as OPD).[49]

SEM and TEM images in Fig. 2 illustrate the morphology of the initial multifaceted geometry of the Fe_3O_4 nanoparticles and Fe_3O_4–Ag nanocomposite. From Fig. 2a and b, it can be seen that the prepared Fe_3O_4 nanoparticles did not have a smooth spherical surface, when compared with common magnetic particles, but instead exhibited an obvious angular multifaceted geometry. As shown in Fig. 2c and d, organized silver nanowires appeared after reduction by oleylamine.[50] The obtained silver nanowires seemed uniform with an average diameter of approximately 40–60 nm with Fe_3O_4 nanoparticles anchored on the surface.

In addition, as shown in Fig. 3, the element mapping results show that the prepared Fe_3O_4–Ag nanocomposite was mainly composed of elements including Ag, O, and Fe. These elemental maps further verify that the Fe_3O_4 nanoparticles were surrounded by Ag nanowires and that Ag nanowires were dispersed homogeneously. To gain more information about the microstructure of the Ag nanowire crystals, high-resolution transmission electron microscopic (HRTEM) analysis was necessary. As shown in Fig. 4a, the obtained Ag nanowire crystal showed a clear crystalline structure and distinct lattice fringe. The interplanar spacing was easily resolved with a value of 0.238 nm, corresponding to the Ag (111) crystal plane. In addition, Fig. 4b demonstrates the XRD pattern of the original Fe_3O_4 nanoparticles compared with that of the Fe_3O_4–Ag nanocomposite. It can be seen from the XRD data that the pattern of the Fe_3O_4 nanoparticles

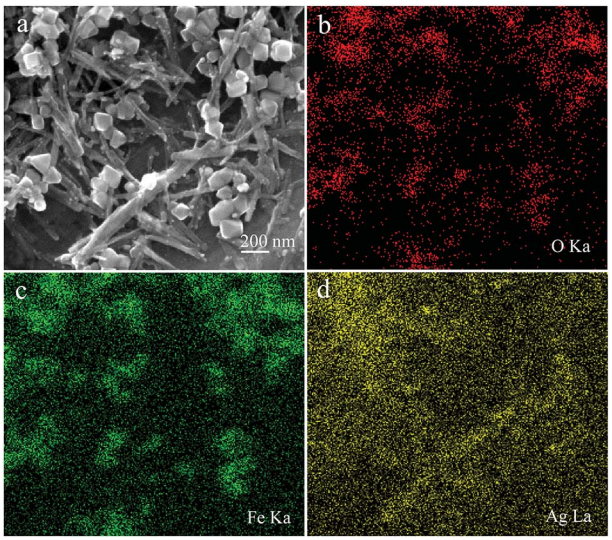

Fig. 3 SEM image (a) and O/Fe/Ag (b, c, and d) elemental mapping of the obtained Fe_3O_4–Ag nanocomposite.

demonstrates characteristic diffraction peaks at 2θ values of 30.1°, 35.4°, 43.0°, 53.4°, 57.1° and 62.2°, which corresponded to the (220), (222), (400), (422), (511) and (440) crystals planes, respectively. These results are in good agreement with the standard card (PDF#88-0315).[51] In previous reports, many similar test results for the diffraction peaks of Fe_3O_4 NPs have been described explicitly.[52–54] As for the pattern of the Fe_3O_4–Ag nanocomposite, obvious diffraction peaks could be observed and indexed to the (111), (200), (220) and (311) planes of pure face-centered cubic (fcc) silver crystals.[55]

Fig. 5 demonstrates the magnetization hysteresis loops of the as-prepared Fe_3O_4 nanoparticles and Fe_3O_4–Ag nanocomposite at room temperature. The saturation magnetization of the prepared Fe_3O_4 nanoparticles was 83.0 emu g^{-1}, which is more than the values reported for other pure Fe_3O_4 nanocrystals.[56–59] In addition, the saturation magnetization value of the Fe_3O_4–Ag nanocomposite was 63.2 emu g^{-1}. These results indicate the successful preparation of the Fe_3O_4–Ag nanocomposite with a coating of Ag nanowires. X-ray photoelectron spectroscopy (XPS) was used to study the surface composition and elemental states in the

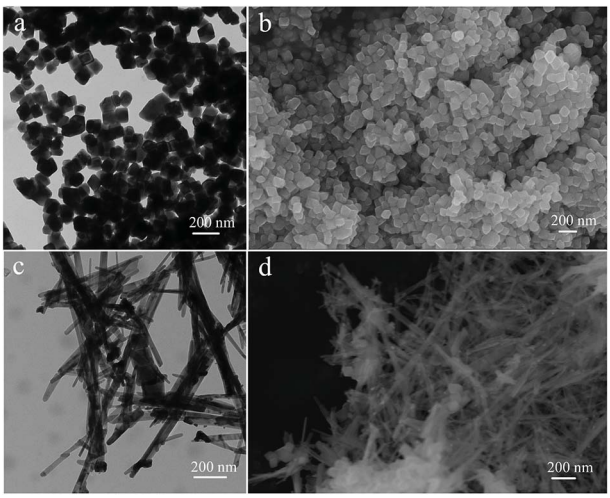

Fig. 2 TEM and SEM images of the prepared Fe_3O_4 nanoparticles (a and b) and Fe_3O_4–Ag nanocomposite (c and d).

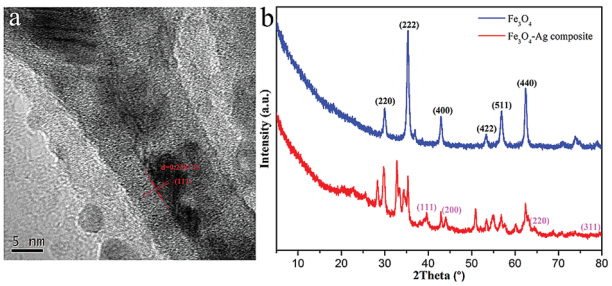

Fig. 4 HRTEM image of Ag nanowires (a) and XRD patterns of the Fe_3O_4–Ag nanocomposite (b).

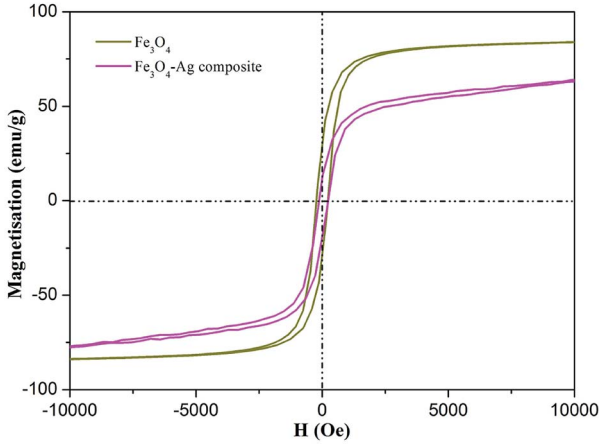

Fig. 5 Magnetization hysteresis loops of as-prepared Fe_3O_4 nanoparticles and Fe_3O_4–Ag nanocomposite.

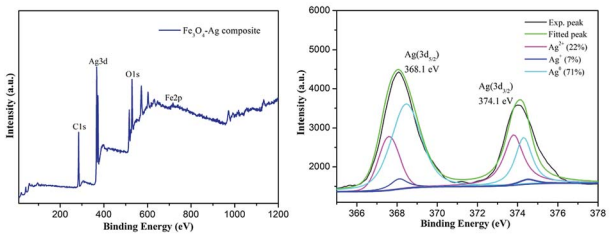

Fig. 6 XPS profiles of the Fe_3O_4–Ag nanocomposite (a) and the deconvolution of Ag peaks (b).

composite.[60–68] As depicted in Fig. 6a, the wide scan of the XPS spectrum showed characteristic peaks of C1s, O1s, Ag3d and Fe2p from the as-prepared Fe_3O_4–Ag nanocomposite. From the deconvolution of Ag peaks in Fig. 6b, two peaks appeared in the Ag(3d) binding energy region. One, located at a binding energy of 368.1 eV, is assigned to the $Ag(3d_{5/2})$ and the other located at 374.1 eV corresponds to $Ag(3d_{3/2})$ with a distance of 6 eV, which may correspond to the $3d_{5/2}$ and $3d_{3/2}$ lines of metallic silver, respectively. Compared with the main Ag^0 (71%) component, the Ag^+ (7%) and Ag^{2+} (22%) content seemed very small, indicating the successful anchoring of the Ag metal onto the obtained composite.

3.2 Catalytic performance

Next, reduction reactions of 4-NP and 2-NA with $NaBH_4$ solution were used to assess the catalytic activity of the as-obtained Fe_3O_4–Ag nanocomposite. $NaBH_4$ provided negative hydrogen ions to attack 4-NP. As shown in Fig. 7, with the process of the classic reduction reaction, the peak of 4-NP at 402 nm decreased gradually, indicating the formation of 4-AP. It can be observed that a period of 70 min was required to finish the reaction. As for the catalytic reduction of 2-NA, after adding the aqueous $NaBH_4$ solution fully, no significant changes in the 2-NA solution were observed in the characteristic absorption peak at 415 nm, as shown in Fig. 7b. However, after adding the Fe_3O_4–

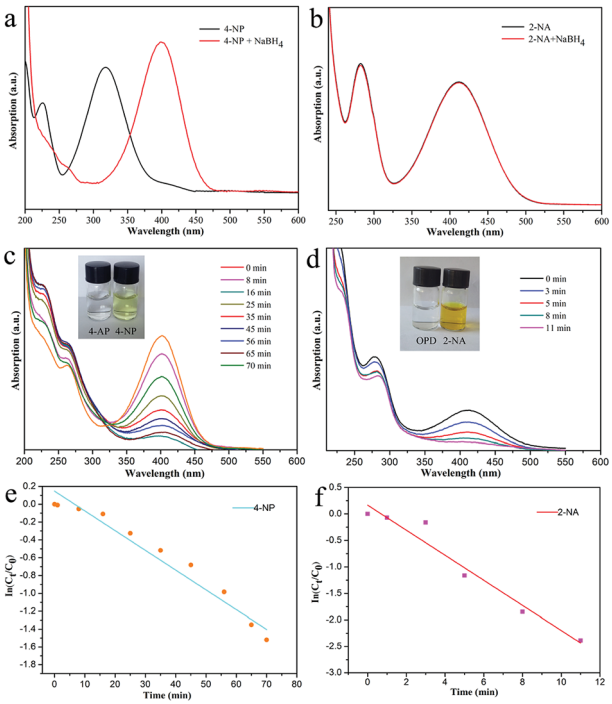

Fig. 7 The spectra of 4-NP and 2-NA with the addition of $NaBH_4$ (a and b). Curves of the catalytic reduction of 4-NP (c) and 2-NA (d). Plots of $\ln(C_t/C_0)$ *versus* time for 4-NP (e) and 2-NA (f). Pictures (insets in (c) and (d)) represent the solutions before/after the catalytic reaction.

Ag composite as a catalyst, the absorption peak of 2-NA was significantly reduced, while the system solution changed from bright yellow to pale yellow to colorless simultaneously after only 11 minutes. Fig. 7e and f depict the linear relationship between $\ln(C_t/C_0)$ and time (t), in which C_0 represents the initial concentration, and C_t represents the concentrations of 4-NP at time t. The pseudo-first-order reaction rate constant (k) was fitted and calculated with the values 0.022 and 0.24 min^{-1} for the reduction reactions of 4-NP and 2-NA, respectively.

For heterogeneous materials to be used in practical applications, their level of reusability and activity in cycling experiments are critical factors. Therefore, in this work, the reusability of the as-prepared Fe_3O_4–Ag catalyst was investigated *via* reduction reactions of 4-NP and 2-NA with fresh $NaBH_4$ solution. The activity of the catalyst was calculated based on the reduction in the reaction rate relative to the initial rate per use. After the catalytic reductions of 4-NP and 2-NA, the Fe_3O_4–Ag composite catalyst could be easily recovered magnetically from the mixed solution and washed with deionized water and ethanol for the next cycle test. Fig. 8 shows the reusability test of the Fe_3O_4–Ag composite over eight successive cycles. The material exhibited a stable catalytic conversion of more than 92%, demonstrating its wide applications in material catalysis and composite design. In addition, as shown in Fig. 9, the morphological and elemental mapping results of the Fe_3O_4–Ag nanocomposite after eight consecutive cycles demonstrate a stable and high dispersion state, highlighting its great potential and high capacity as a new catalyst.

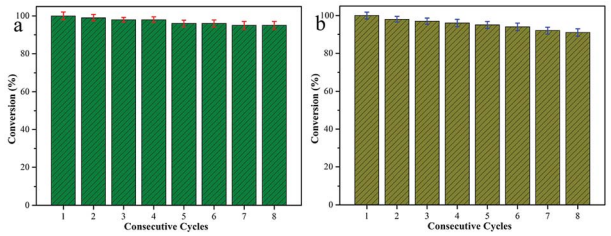

Fig. 8 Reusability test of the present Fe_3O_4–Ag nanocomposite as a catalyst for the reduction of 4-NP (a) and 2-NA (b) for eight consecutive cycles.

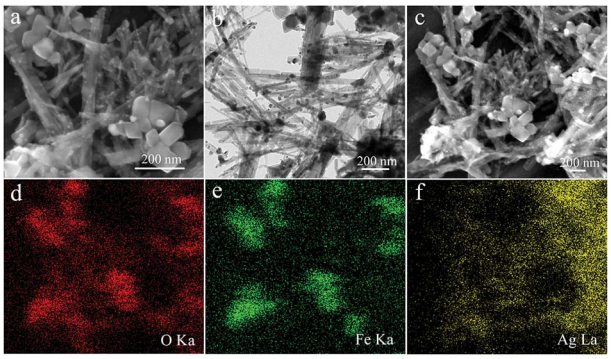

Fig. 9 SEM (a) and TEM (b) images with O/Fe/Ag elemental mapping (d, e, and f) of the Fe_3O_4–Ag nanocomposite after eight consecutive cycles of catalytic reactions.

4. Conclusions

In summary, we have successfully synthesized a Fe_3O_4–Ag nanocomposite material *via* a solvothermal method. A series of characterization techniques revealed that Ag nanowires were successfully anchored onto Fe_3O_4 nanoparticles. The synthesized Fe_3O_4–Ag composite showed excellent catalytic activity for the reduction of 4-NP and 2-NA in the presence of $NaBH_4$. It is interesting to note that the as-synthesized Fe_3O_4–Ag composite catalyst demonstrated good reusability even after eight cycles at room temperature. Thus, the as-prepared composite catalyst, with superior catalytic ability, convenient magnetic separation capability and excellent reusability, is expected to have great potential as a magnetic functional composite for various advanced catalytic applications.

Conflicts of interest

There are no conflicts to declare.

Acknowledgements

We greatly appreciate the financial supports of National Natural Science Foundation of China (No. 21872119, 21473153, and 51771162), Support Program for the Top Young Talents of Hebei Province, China Postdoctoral Science Foundation (No. 2015M580214), Research Program of the College Science & Technology of Hebei Province (No. ZD2018091), and Scientific and Technological Research and Development Program of Qinhuangdao City (No. 201701B004).

Notes and references

1 W. Che, Y. Ni, Y. Zhang and Y. Ma, *J. Phys. Chem. Solids*, 2015, **77**, 1–7.
2 Z. Dong, X. Le, X. Li, W. Zhang and C. Dong, *Appl. Catal., B*, 2014, **158–159**, 129–135.
3 H. Saikia, B. J. Borah, Y. Yamada and P. Bharali, *J. Colloid Interface Sci.*, 2017, **486**, 46–57.
4 R. Guo, T. Jiao, R. Li, Y. Chen, W. Guo, L. Zhang, J. Zhou, Q. Zhang and Q. Peng, *ACS Sustainable Chem. Eng.*, 2018, **6**, 1279–1288.
5 S. Xuan, F. Wang and J. M. Y. Lai, *ACS Appl. Mater. Interfaces*, 2011, **3**, 237–244.
6 D. Zhang, Z. Liu, S. Han, C. Li and B. Lei, *Nano Lett.*, 2004, **4**, 2151–2155.
7 Y. Zhan, R. Zhao, Y. Lei, F. Meng and J. Zhong, *J. Magn. Magn. Mater.*, 2011, **323**, 1006–1010.
8 J. S. Xu and Y. J. Zhu, *ACS Appl. Mater. Interfaces*, 2012, **4**, 4752–4757.
9 A. H. Lu, W. Schmidt, N. Matoussevitch, H. Boennemann and B. Spliethoff, *Angew. Chem., Int. Ed.*, 2004, **43**, 4303–4306.
10 Y. Zhu, Y. Fang and S. Kaskel, *J. Phys. Chem. C*, 2010, **114**, 16382–16388.
11 Y. Chen, H. Chen, D. Zeng, Y. Tian and F. Chen, *ACS Nano*, 2010, **4**, 6001–6013.
12 S. Linley, T. Leshuk and F. X. Gu, *ACS Appl. Mater. Interfaces*, 2013, **5**, 2540–2548.
13 Y. Liu, Y. Wang, S. Zhou, S. Lou and L. Yuan, *ACS Appl. Mater. Interfaces*, 2012, **4**, 4913–4920.
14 Q. Cheng, F. Qu, N. B. Li and H. Q. Luo, *Anal. Chim. Acta*, 2012, **715**, 113–119.
15 Y. Sun and C. Lei, *Angew. Chem., Int. Ed.*, 2010, **48**, 6824–6827.
16 S. Xie, N. Lu, Z. Xie, J. Wang and M. J. Kim, *Angew. Chem., Int. Ed.*, 2012, **124**, 10412–10416.
17 Y. Li and W. J. Shen, *Sci. China: Chem.*, 2012, **55**, 2485–2496.
18 N. Tian, Z. Y. Zhou, S. G. Sun, Y. Ding and Z. L. Wang, *Science*, 2007, **38**, 732–735.
19 A. R. Tao, S. Habas and P. Yang, *Small*, 2010, **4**, 310–325.
20 S. Yang, Z. Peng and H. Yang, *Adv. Funct. Mater.*, 2008, **18**, 2745–2753.
21 J. Jiu, T. Sugahara, M. Nogi and K. Suganuma, *J. Nanopart. Res.*, 2013, **15**, 1–13.
22 A. Manivannan, G. Glaspell and M. S. Seehra, *J. Appl. Phys.*, 2003, **94**, 6994–6996.
23 B. H. Hong, S. C. Bae, C. W. Lee, S. Jeong and K. S. Kim, *Science*, 2001, **294**, 348–351.
24 X. Zhang, M. A. Young, O. Lyandres and R. P. Van Duyne, *J. Am. Chem. Soc.*, 2005, **127**, 4484–4489.
25 J. L. West and N. J. Halas, *Annu. Rev. Biomed. Eng.*, 2003, **5**, 285–292.

26 C. J. Murphy, A. M. Gole, J. W. Stone, P. N. Sisco and A. M. Alkilany, *Acc. Chem. Res.*, 2008, **40**, 1721–1730.
27 K. Li, T. Jiao, R. Xing, G. Zou, J. Zhou, L. Zhang and Q. Peng, *Sci. China Mater.*, 2018, **61**, 728–736.
28 H. Gao, Y. Li, C. Li, F. Ma, Z. Song and K. Xu, *RSC Adv.*, 2016, **6**, 30998–31004.
29 L. Wang, A. Shen, X. Li, Y. Zeng, X. Zhou, R. M. Richards and J. Hu, *RSC Adv.*, 2014, **4**, 34294–34302.
30 J. Hu, S. Wu, Q. Cao and W. Zhang, *RSC Adv.*, 2016, **6**, 81767–81773.
31 Q. Wang, X. Zhao, X. K. Zhang, Y. I. Lee and H. G. Liu, *RSC Adv.*, 2015, **5**, 69339–69347.
32 A. Barrera, F. Tzompantzi, J. Campa-Molina, J. E. Casillas, R. Pérez-Hernández, S. Ulloa-Godinez, C. Velasquez and J. Arenas-Alatorre, *RSC Adv.*, 2018, **8**, 3108–3119.
33 P. Gnanaprakasam and T. Selvaraju, *RSC Adv.*, 2014, **4**, 24518–24525.
34 T. Jiao, Y. Liu, Y. Wu, Q. Zhang, X. Yan, F. Gao, A. J. P. Bauer, J. Liu, T. Zeng and B. Li, *Sci. Rep.*, 2015, **5**, 12451.
35 Y. Liu, C. Hou, T. Jiao, J. Song, X. Zhang, R. Xing, J. Zhou, L. Zhang and Q. Peng, *Nanomaterials*, 2018, **8**, 35.
36 W. Guo, Q. Wang, G. Wang, M. Yang and W. Dong, *Chem.–Asian J.*, 2013, **8**, 1160–1167.
37 W. Guo, J. Jiao, K. Tian and Y. Tang, *RSC Adv.*, 2015, **5**, 102210–102218.
38 M. Liang, R. Su, W. Qi, Y. Yu and L. Wang, *J. Mater. Sci.*, 2014, **49**, 1639–1647.
39 W. Guo, Q. Wang, Y. Luan, G. Wang and W. Dong, *Chem.–Asian J.*, 2015, **10**, 701–708.
40 S. Peng, F. Gao, D. Zeng, C. Peng and Y. Chen, *Cellulose*, 2018, **25**, 1–12.
41 Z. Sun, H. Li, G. Cui, Y. Tian and S. Yan, *Appl. Surf. Sci.*, 2016, **360**, 252–262.
42 Q. Du, L. Tan, B. Li, T. Liu and J. Ren, *RSC Adv.*, 2014, **4**, 56057–56062.
43 Y. Liu, Y. Y. Zhang, Q. W. Kou, Y. Chen and D. L. Han, *RSC Adv.*, 2018, **8**, 2209–2218.
44 U. Kurtan, E. Onuş, Md. Amir and A. Baykal, *J. Inorg. Organomet. Polym.*, 2015, **25**, 1120–1128.
45 S. Huo, P. Duan, T. Jiao, Q. Peng and M. Liu, *Angew. Chem., Int. Ed.*, 2017, **56**, 12174–12178.
46 Q. Han, Z. Wang, J. Xia, S. Chen and X. Zhang, *Talanta*, 2012, **101**, 388–395.
47 X. Du, P. Guo, H. Song and X. Chen, *Electrochim. Acta*, 2010, **55**, 4812–4819.
48 X. Zhao, T. Jiao, R. Xing, H. Huang and J. Hu, *RSC Adv.*, 2017, **7**, 49923–49930.
49 H. Shi, C. Zhou and C. Zhang, *Res. Chem. Intermed.*, 2015, **41**, 1–13.
50 H. Wang, J. Deng, Y. Chen, F. Xu and Z. Wei, *Nano Res.*, 2016, **9**, 1–9.
51 L. Sun, X. Hong, P. Zou, X. Chu and Y. Liu, *J. Alloys Compd.*, 2012, **535**, 91–94.
52 X. Zhou, Y. Shi, L. Ren, S. Bao and Y. Han, *J. Solid State Chem.*, 2012, **196**, 138–144.
53 G. Basina, G. Mountrichas, E. Devlin, N. Boukos and D. Niarchos, *J. Nanosci. Nanotechnol.*, 2009, **9**, 4753–4759.
54 D. Chen, X. Qiao, X. Qiu, J. Chen and R. Jiang, *J. Colloid Interface Sci.*, 2010, **344**, 286–291.
55 P. Hervés, M. Pérez-Lorenzo, L. M. Liz-Marzán, J. Dzubiella and Y. Lu, *Chem. Soc. Rev.*, 2012, **41**, 5577–5587.
56 J. Zhou, Y. Liu, T. Jiao, R. Xing, Z. Yang, J. Fan, J. Liu, B. Li and Q. Peng, *Colloids Surf., A*, 2018, **538**, 7–13.
57 J. Zhou, F. Gao, T. Jiao, R. Xing, L. Zhang, Q. Zhang and Q. Peng, *Colloids Surf., A*, 2018, **545**, 60–67.
58 X. Luo, K. Ma, T. Jiao, R. Xing, L. Zhang, J. Zhou and B. Li, *Nanoscale Res. Lett.*, 2017, **12**, 99.
59 K. Chen, J. Li, L. Zhang, R. Xing, T. Jiao, F. Gao and Q. Peng, *Nanotechnology*, 2018, **29**, 445603.
60 R. Xing, K. Liu, T. Jiao, N. Zhang, K. Ma, R. Zhang, Q. Zou, G. Ma and X. Yan, *Adv. Mater.*, 2016, **28**, 3669–3676.
61 H. Guo, T. Jiao, Q. Zhang, W. Guo, Q. Peng and X. Yan, *Nanoscale Res. Lett.*, 2015, **10**, 272.
62 R. Xing, W. Wang, T. Jiao, K. Ma, Q. Zhang, W. Hong, H. Qiu, J. Zhou, L. Zhang and Q. Peng, *ACS Sustainable Chem. Eng.*, 2017, **5**, 4948–4956.
63 X. Zhao, K. Ma, T. Jiao, R. Xing, X. Ma, J. Hu, H. Huang, L. Zhang and X. Yan, *Sci. Rep.*, 2017, **7**, 44076.
64 J. Song, R. Xing, T. Jiao, Q. Peng, C. Yuan, H. Möhwald and X. Yan, *ACS Appl. Mater. Interfaces*, 2018, **10**, 2368–2376.
65 X. Huang, T. Jiao, Q. Liu, L. Zhang, J. Zhou, B. Li and Q. Peng, *Sci. China Mater.*, 2019, **62**, 423–436.
66 C. Wang, S. Sun, L. Zhang, J. Yin, T. Jiao, L. Zhang, Y. Xu, J. Zhou and Q. Peng, *Colloids Surf., A*, 2019, **561**, 283–291.
67 S. Sun, C. Wang, S. Han, T. Jiao, R. Wang, J. Yin, Q. Li, Y. Wang, L. Geng, X. Yu and Q. Peng, *Colloids Surf., A*, 2019, **564**, 1–9.
68 Y. Xu, B. Ren, R. Wang, L. Zhang, T. Jiao and Z. Liu, *Nanomaterials*, 2019, **9**, 10.